Maximal slicing of *D*-dimensional spherically symmetric vacuum spacetime

Ken-ichi Nakao,[1,*] Hiroyuki Abe,[1,†] Hirotaka Yoshino,[2,‡] and Masaru Shibata[3,§]

[1]*Department of Mathematics and Physics, Graduate School of Science, Osaka City University, Osaka 558-8585, Japan*
[2]*Department of Physics, University of Alberta, Edmonton, Alberta, Canada T6G 2G7*
[3]*Yukawa Institute for Theoretical Physics, Kyoto University, Kyoto 606-8502, Japan*

We study the foliation of a *D*-dimensional spherically symmetric black-hole spacetime with $D \geq 5$ by two kinds of one-parameter families of maximal hypersurfaces: a reflection-symmetric foliation with respect to the wormhole slot and a stationary foliation that has an infinitely long trumpetlike shape. As in the four-dimensional case, the foliations by the maximal hypersurfaces avoid the singularity irrespective of the dimensionality. This indicates that the maximal slicing condition will be useful for simulating higher-dimensional black-hole spacetimes in numerical relativity. For the case of $D = 5$, we present analytic solutions of the intrinsic metric, the extrinsic curvature, the lapse function, and the shift vector for the foliation by the stationary maximal hypersurfaces. These data will be useful for checking five-dimensional numerical-relativity codes based on the moving puncture approach.

I. INTRODUCTION

The merger of binary black holes is one of the most important sources of gravitational waves for gravitational-wave detectors. As a result of long-term efforts by many numerical-relativity researchers, it is now feasible to theoretically predict the late stages of the orbital evolution and merger process of astrophysical binary black holes and resulting gravitational waves emitted from these systems by numerical relativity. After the first report of long-term simulations of binary black holes by Pretorius [1], several groups have also succeeded in long-term simulations [2–7]. There are basically three formulations of numerical relativity for simulating a dynamical black-hole system; one is the "generalized harmonic" formulation with the help of "black-hole excision" [1], the second one is the so-called Baumgarte-Shapiro-Shibata-Nakamura (BSSN) formulation [8,9] together with the "moving puncture" method, and the third one is the hyperbolic formulation with the black-hole excision [6]. Among the three different approaches, the BSSN formalism is currently most widely used, because of its simplicity in implementing numerical code.

Another scenario of black-hole formation in the system of two relativistic objects was pointed out in the nonastrophysical context [10–12]: mini-black-hole production at high-energy particle collisions in particle accelerators in the framework of the brane world scenarios (i.e., the so-called TeV gravity scenarios) [13,14]. Motivated by this possibility, mini black holes in the particle colliders have

been studied by many researchers in the past decade from a wide variety of viewpoints (see [15] for a recent review). There are two marked differences between the black-hole production in the colliders and the black-hole mergers in astrophysical situations. One is the relative speed of the objects. In the high-energy particle collisions at the LHC, the γ factor of an incoming proton is $\sim 7 \times 10^3$, and that of its constituent partons can be much larger. The other is the number *D* of the spacetime dimensions, because a spacetime dimension higher than four is essential for the TeV gravity scenarios.

In order to understand well the black-hole production in the particle colliders, numerical relativity is probably the unique approach, since this issue is a highly nonlinear phenomenon. To perform a simulation of this system, two techniques have to be developed: One is the technique to handle the high-energy objects, and the other to simulate higher-dimensional black-hole spacetimes. The first technique has been developed for the four-dimensional case [16–18] by modeling the high-energy two-particle system as the high-velocity two-black-hole collision and extrapolating the results to the ultrarelativistic regime. Such simulations have not been performed for higher-dimensional spacetimes yet (but see Refs. [19,20] for studies on the apparent horizon in the system of two high-energy particles in higher dimensions). Also, a numerical code to simulate higher-dimensional spacetimes with the BSSN formalism has been recently developed [21] (see a list of proposed several test simulations and the successful results).

Usually, in numerical relativity, the four-dimensional Einstein equations are written in the form of evolution and constraint equations for geometrical quantities of three-dimensional space with some conditions to deter-

*knakao@sci.osaka-cu.ac.jp
†abe@sci.osaka-cu.ac.jp
‡hyoshino@phys.ualberta.ca
§shibata@yukawa.kyoto-u.ac.jp

mine the coordinate system. Then numerical integrations of the evolution equations lead to a solution of four-dimensional spacetime with a foliation by spacelike hypersurfaces labeled by the time coordinate. There is large freedom in choosing a foliation, and, if the foliation is appropriate for the subject of our interest, the numerical simulations give us information about a sufficiently wide domain of the spacetime.

The maximal slicing is a foliation by a one-parameter family of the spacelike hypersurface with vanishing mean extrinsic curvature and is known as one of the workable slicing conditions in four-dimensional numerical simulations for astrophysical situations. Thus, in this paper, we investigate the maximal slicing condition for the D-dimensional spherically symmetric black-hole spacetime ($D \geq 5$), known as the Schwarzschild-Tangherlini solution [22]. This study is motivated by numerical relativity performed with the BSSN formalism and the puncture method, by which a whole spacetime region including the black-hole interior is simulated, and, thus, the slicing condition that avoids the singularity has to be adopted. For the four-dimensional Schwarzschild black hole, it was shown that the sequence of maximal slices never plunges into the curvature singularity but asymptotes to the so-called limit surface which exists inside the event horizon [23]. We shall show that the sequence of the maximal slices avoids the singularity also in the higher-dimensional Schwarzschild-Tangherlini spacetime. This gives the theoretical foundation that both the maximal slicing condition and the puncture gauge condition (see [24,25]) have the desired features in higher-dimensional numerical relativity. Another important aspect of this study is to derive a stationary sequence of the maximal slicing hypersurfaces that provides a useful analytic solution for a benchmark test of higher-dimensional numerical-relativity codes, as discussed in Refs. [25,26] in the four-dimensional case.

This paper is organized as follows. In Sec. II, we derive the general solution in the maximal slicing for the D-dimensional spherically symmetric black-hole spacetime. Then, in Sec. III, we investigate the foliation by the maximal hypersurfaces which are reflection-symmetric at the wormhole slot. In Sec. IV, we study the foliation by the stationary maximal hypersurfaces. After explicitly describing the analytic solution in the case $D = 5$, we show its usefulness as a benchmark test for numerical relativity, by performing a numerical simulation adopting the analytic solution as the initial data. Section V is devoted to a summary. In the appendix, the Kruskal extension of the Schwarzschild-Tangherlini spacetime is analyzed.

We adopt the geometrized units $c = G = 1$ throughout this paper, where c is the speed of light and G is the gravitational constant of a D-dimensional spacetime. The Greek indices ($\mu, \nu, \dots$) represent the components of a spacetime, while the Latin indices ($i, j, \dots$) represent the components of a space.

II. GENERAL SPHERICALLY SYMMETRIC MAXIMAL SLICING

Following Estabrook *et al.* [23], we derive general spherically symmetric maximal slicing of the Schwarzschild-Tangherlini spacetime, i.e., the D-dimensional spherically symmetric vacuum black-hole solution with $D \geq 5$. The general form of its line element is

$$ds^2 = -\alpha^2 dt^2 + \gamma(dr + \gamma^{-1}\beta dt)^2 + r^2 d\Omega_{D-2}^2, \quad (1)$$

where $d\Omega_{D-2}^2$ is the line element of a $(D-2)$-dimensional unit sphere with the $(D-2)$ area $\Omega_{D-2} := (D-1)\pi^{(D-1)/2}/\Gamma(\frac{D+1}{2})$ and α, β, and γ are functions of t and r.

Einstein's equations with appropriate coordinate conditions lead to the basic equations for α, β, and γ. Because the $(D-2)$-dimensional spherical-polar coordinate system is uniquely determined in the spherically symmetric spacetime, two conditions are required to fix the remaining two coordinates: the condition to determine the foliation of the spacetime by a one-parameter family of spacelike hypersurfaces and that to specify the time evolution of the radial coordinate. In Eq. (1), the radial coordinate has already been fixed so that $\Omega_{D-2}r^{D-2}$ becomes the area of the $(D-2)$-dimensional sphere labeled by r. Thus, we need only the condition for the foliation. As mentioned earlier, we shall consider the foliation of this spacetime by the family of maximal hypersurfaces, where a maximal hypersurface implies that the trace of the extrinsic curvature vanishes on it, i.e., $K = 0$.

In the following, we solve Einstein's equations for the metric (1) in the maximal slicing condition. From the maximal slicing condition $K = 0$, we have

$$-\partial_t(\ln\gamma) + \beta\gamma^{-1}\partial_r[\ln(\beta^2\gamma^{-1}r^{2(D-2)})] = 0. \quad (2)$$

The Hamiltonian and momentum constraints are calculated to give

$$(D-1)\alpha^{-2}\beta^2\gamma^{-1} = (D-3)(\gamma-1) + r\partial_r(\ln\gamma), \quad (3)$$

$$\partial_r[\ln(\alpha^{-1}\beta\gamma^{-1}r^{D-2})] = 0. \quad (4)$$

By using $\partial_t K = 0$, the evolution equation for the trace part of the extrinsic curvature reduces to

$$\partial_r^2\alpha + (D-2)r^{-1}\partial_r\alpha - \tfrac{1}{2}[\partial_r(\ln\gamma)]\partial_r\alpha$$
$$= (D-2)r^{-2}[(D-3)(\gamma-1) + r\partial_r(\ln\gamma)]. \quad (5)$$

The remaining nontrivial component of the evolution equations gives

$$\partial_t[\ln(\alpha^{-1}\beta)] = [(2D-5)\beta\gamma^{-1}$$
$$+ (D-3)\alpha^2\beta^{-1}(\gamma-1)]r^{-1} + 3\gamma^{-1}\partial_r\beta$$
$$+ \tfrac{1}{2}(\alpha^2\beta^{-1} - 4\beta\gamma^{-1})\partial_r(\ln\gamma)$$
$$- (\beta\gamma^{-1} + \alpha^2\beta^{-1})\partial_r(\ln\alpha). \quad (6)$$

General solutions for α, β, and γ are derived as follows. From Eq. (4), β is determined as

$$\beta = T(t)\alpha\gamma r^{-(D-2)}, \quad (7)$$

where $T(t)$ is a function of integration. By substituting the above equation into Eq. (3), the equation for γ is derived to give

$$\partial_r(r^{D-3}\gamma^{-1}) = (D-3)r^{D-4} - (D-1)T^2 r^{-D}, \quad (8)$$

and by the integration of this equation, we obtain

$$\gamma^{-1} = 1 - [r_g(t)/r]^{D-3} + T^2/r^{2(D-2)}, \quad (9)$$

where $r_g(t)$ is a function of integration. Eliminating β in Eq. (2) by using Eq. (7), and then using Eq. (9), we have

$$\partial_r(\alpha\gamma^{1/2}) = \gamma^{3/2}\left[\frac{\partial_t(r_g^{D-3})r}{2T} - \frac{\partial_t T}{r^{D-2}}\right]. \quad (10)$$

Eliminating β from Eq. (6) and rewriting the result with help of Eq. (10), we find that r_g is a constant:

$$\partial_t r_g = 0. \quad (11)$$

By using this fact, Eq. (10) is integrated to give

$$\alpha = f(r_g/r;T)^{1/2}\left[1 + \frac{\partial_t T}{r_g^{D-3}}\int_0^{r_g/r} x^{D-4}f(x;T)^{-3/2}dx\right], \quad (12)$$

where

$$f(x;T) := 1 - x^{D-3} + T^2 r_g^{-2(D-2)}x^{2(D-2)}. \quad (13)$$

If $T(t)$ is determined, γ and α are subsequently derived by solving Eqs. (9) and (12), and then β is determined by Eq. (7). Because $T(t)$ is an arbitrary function, we have to impose an additional condition for $T(t)$ for specifying a solution. In the next section, we impose the reflection symmetry with respect to the wormhole slot and derive the function $T(t)$ that specifies this slicing. In Sec. IV, we also consider the case that $T(t)$ is constant and give a different class of the maximal hypersurfaces.

III. REFLECTION-SYMMETRIC FOLIATION

The coordinate system with the choice $T = 0$ agrees with the Schwarzschild-Tangherlini static coordinates:

$$ds^2 = -\left[1 - \left(\frac{r_g}{r}\right)^{D-3}\right]d\tau^2 + \left[1 - \left(\frac{r_g}{r}\right)^{D-3}\right]^{-1}dr^2 + r^2 d\Omega_{D-2}^2. \quad (14)$$

To derive the coordinates for the general foliation with $T \neq 0$, we first prepare the maximally extended Schwarzschild-Tangherlini spacetime (see the appendix for the Kruskal extension) and then perform coordinate transformation from the Schwarzschild-Tangherlini coordinates (τ, r) to the coordinates (t, r) for a foliation $T \neq 0$. Here the Schwarzschild-Tangherlini time coordinate τ is given as

$\tau = \tau(t, r)$ and satisfies

$$\frac{\partial\tau}{\partial t} = \alpha\gamma^{1/2}, \quad (15)$$

$$\frac{\partial\tau}{\partial r} = -\gamma^{1/2}Tr^{-(D-2)}\left[1 - \left(\frac{r_g}{r}\right)^{D-3}\right]^{-1}. \quad (16)$$

Integrating Eq. (16) gives τ in the form

$$\tau = Tr_g^{-D+3}\int_{r_g/r}^{X(T)}\frac{x^{D-4}}{(x^{D-3}-1)f(x;T)^{1/2}}dx, \quad (17)$$

where $X(T)$ is a function of integration. By substituting the above equation into Eq. (15), the equation for X is derived as

$$\frac{dX}{dT} = T^{-1}X^{4-D}(X^{D-3}-1)f(X;T)^{1/2}$$
$$\times\left[\frac{r_g^{D-3}}{\partial_t T} + \int_0^X \frac{x^{D-4}}{f(x;T)^{3/2}}dx\right]. \quad (18)$$

Here we require the hypersurface to have a reflection symmetry with respect to the wormhole slot, i.e., $\tau = 0$, which is located in the black-hole interior $r = r_{\min} < r_g$ (see the Kruskal diagram in Fig. 1); this condition determines $T(t)$. At $\tau = 0$, the 1-form $\nabla_\mu t$, normal to the
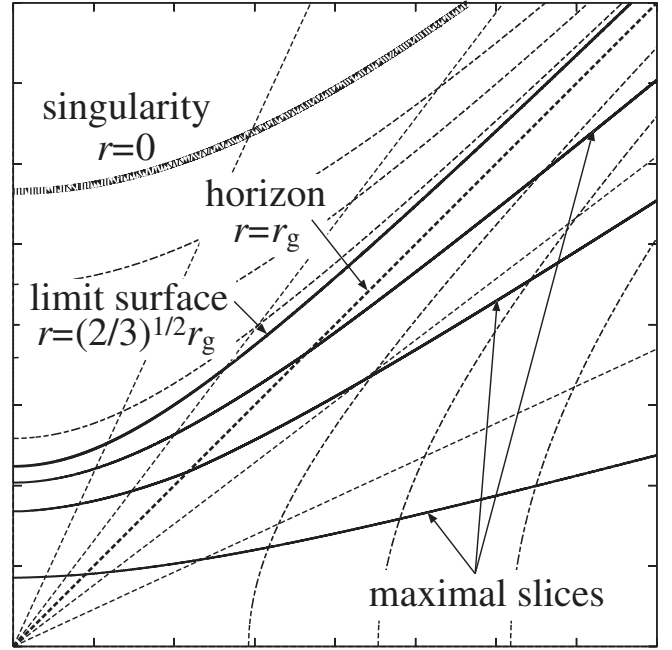

FIG. 1. The reflection-symmetric maximal slicing in the Kruskal diagram of Schwarzschild-Tangherlini spacetime with $D = 5$. The maximal hypersurfaces with the reflection symmetry with respect to the wormhole slot $\tau = 0$ are depicted by solid curves. The dotted curves show the $r = \mathrm{const}$ lines, while the dotted straight lines indicate the $\tau = \mathrm{const}$ lines. The singularity, the limit surface, and the horizon are given by $r = 0$, $\sqrt{2/3}r_g$, and r_g, respectively.

hypersurface labeled by t, should be perpendicular to $(\partial/\partial\tau)^\mu$ because τ is a spacelike coordinate in the black-hole interior, and thus

$$\left(\frac{\partial}{\partial\tau}\right)^\mu \nabla_\mu t = \frac{1}{\alpha\gamma^{1/2}} = 0 \quad \text{at } \tau = 0. \qquad (19)$$

Because α should be finite everywhere on the slice, the following condition has to be satisfied:

$$\frac{1}{\gamma(r_{\min}; T)} = 0. \qquad (20)$$

Note that the circumferential radius r takes the minimal value $r_{\min}$ at $\tau = 0$ in the black-hole interior because of the requirement of the reflection symmetry. Equation (20) determines the value of $r_{\min}$ for a given value of T, i.e., $r_{\min} = r_{\min}(T)$.

The equation $f(x; T) = 0$ has at most two real positive roots, and the smaller one is $x = r_g/r_{\min}$ because $f(r_g/r; T) = 1/\gamma(r; T)$ holds. By a careful limiting procedure, the following fact is found: If $X(T)$ is a smaller root of $f(X; T) = 0$, then X satisfies Eq. (18); if X is a larger root, then the integrand in Eq. (18) becomes imaginary which is unphysical. This implies that we have to adopt $X(T) = r_g/r_{\min}(T)$ in Eq. (17).

We further require the time coordinate t to agree with the Schwarzschild-Tangherlini time coordinate τ at spacelike infinity $r \to \infty$. Then Eq. (17) gives

$$t = T r_g^{-D+3} \int_0^{X(T)} \frac{x^{D-4}}{(x^{D-3} - 1)\sqrt{f(x; T)}} dx. \qquad (21)$$

This equation determines the function of $T(t)$.

If the equation $f(x, T) = 0$ has a degenerate double root, the integral of Eq. (21) diverges, i.e., $t = \infty$. This is the so-called limit surface to which the sequence of maximal hypersurfaces asymptotes. Since the root of $f = 0$ is also the root of the equation $df/dx = 0$ in this case, we obtain

$$\lim_{t\to\infty} T^2(t) = T_\infty^2$$
$$:= \frac{D-3}{2(D-2)}\left[\frac{D-1}{2(D-2)}\right]^{(D-1)/(D-3)} r_g^{2(D-2)}. \qquad (22)$$

The root $x = x_{\lim}$ of $f(x, T_\infty) = 0$ is then given by

$$x_{\lim} = \left[\frac{2(D-2)}{D-1}\right]^{1/(D-3)}. \qquad (23)$$

The minimal radius $r_{\min}$ for $t \to \infty$ is called the limit radius, and it is given by

$$r_{\lim} = \frac{r_g}{x_{\lim}} = \left[\frac{D-1}{2(D-2)}\right]^{1/(D-3)} r_g. \qquad (24)$$

In the case of $D = 4$, this shows the known result $r_{\lim} = (3/4)r_g$ [23].

Several maximal hypersurfaces with the reflection symmetry at the wormhole slot $\tau = 0$ for the case of $D = 5$ are depicted in the Kruskal diagram in Fig. 1 (see the appendix for the method of embedding). As in the case $D = 4$, the sequence of maximal hypersurfaces avoids the singularity for $D \geq 5$.

IV. STATIONARY FOLIATION

In this section, we turn our attention to a foliation of maximal hypersurfaces which is different from the one analyzed in Sec. III: foliations for which $T(t)$ is constant and the reflection symmetry with respect to the wormhole slot is not imposed in general. As the fixed value, we choose $T = T_\infty$ defined in Eq. (22). In this case, the sequence of hypersurfaces is the one-parameter family labeled by t (not by T), and the metric does not depend on the time coordinate t. Because the time coordinate basis is not orthogonal to each hypersurface, we refer to this foliation as the stationary foliation.

Several stationary maximal hypersurfaces of $T = T_\infty$ for $D = 5$ are depicted in the Kruskal diagram in Fig. 2 (see the appendix for the method of embedding). The limit surface exists also for the stationary foliation with $T = T_\infty$, and it agrees with the limit surface of the reflection-symmetric foliation, studied in the previous section. Figure 2 shows that the sequence of maximal hypersurfaces in this class also avoids the singularity and that, except
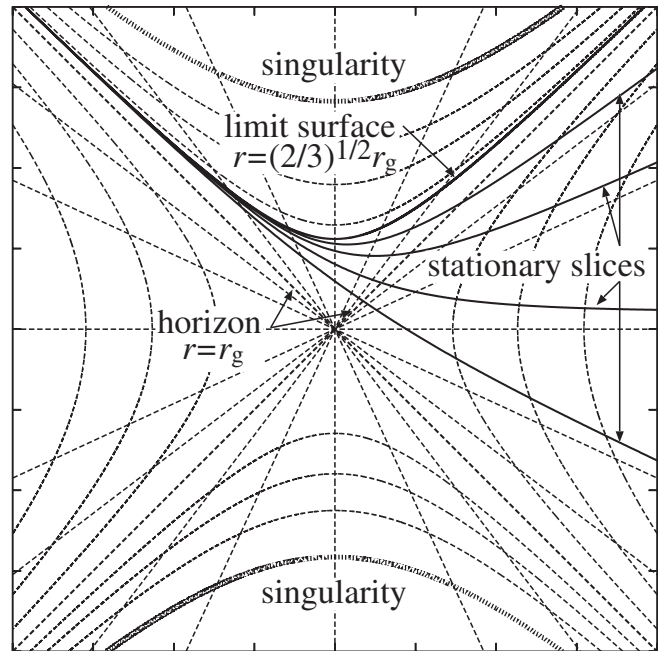

FIG. 2. The stationary maximal slicings of $T = T_\infty$ in the Kruskal diagram of Schwarzschild-Tangherlini spacetime with $D = 5$ (solid lines). Except for the limit surface $r = \sqrt{2/3}r_g$, the maximal hypersurfaces of $T = T_\infty$ are not symmetric with respect to the wormhole slot.

for the limit surface, the hypersurfaces of the stationary foliation are not reflection-symmetric.

The stationary foliation is of special interest in connection with numerical relativity performed in the moving puncture approach, because it would be an attractor of the time evolution with a dynamical slicing ($\partial_t \alpha = -C\alpha K$, where C is a constant) [27] and Γ-driver conditions [24] as demonstrated in [25] for $D = 4$ and in [21] for $D = 5$. In other words, the numerical evolution starting from a hypersurface of stationary foliation has to remain unchanged in time in these gauge conditions. Therefore, this solution provides a useful benchmark test for higher-dimensional numerical-relativity codes.

Black-hole simulation in numerical relativity is often performed in the isotropic coordinates. In Sec. IV A, we describe hypersurfaces of stationary foliation in the isotropic coordinates and study the asymptotic behaviors of the spatial metric. In Sec. IV B, we derive the analytic solution of the stationary maximal hypersurface for $D = 5$ in terms of the BSSN variables and then demonstrate its usefulness for a benchmark test of numerical-relativity codes, by performing numerical simulation.

A. Asymptotic behaviors

In the isotropic coordinates, the line element of a $(D - 1)$-dimensional spherically symmetric spacelike hypersurface is written as

$$dl^2 = \psi^{4/(D-3)}(dR^2 + R^2 d\Omega_{D-2}).\qquad(25)$$

By comparing this with the spatial part of the metric (1), the relation between the coordinates r and R is found:

$$\gamma^{1/2} dr = \psi^{2/(D-3)} dR,\qquad(26)$$

$$r = \psi^{2/(D-3)} R.\qquad(27)$$

These equations lead to a differential equation

$$\frac{d\ln R}{d\ln r} = \frac{1}{\sqrt{f(r_g/r; T_\infty)}},\qquad(28)$$

and the formal solution is given by

$$R = R_c e^{I(r)},\qquad(29)$$

where

$$I(r) = \int_{r_g/r}^1 \frac{dx}{x\sqrt{f(x; T_\infty)}}.\qquad(30)$$

In the following, we analyze asymptotic relations between r and R and the behavior of the conformal factor ψ in the distant region $r \gg r_g$ and in the neighborhood of $r = r_{\text{lim}}$ [given by Eq. (24)], one by one.

In order to study the asymptotic behavior of R in the distant region, we rewrite the function $I(r)$ in the form

$$I(r) = -\ln(r_g/r) + F(r_g/r),\qquad(31)$$

where

$$F(y) := \int_y^1 dx \frac{1 - \sqrt{f(x; T_\infty)}}{x\sqrt{f(x; T_\infty)}}.\qquad(32)$$

For analyzing its behavior for $y \to 0$, we write $F(y)$ in the form of a Maclaurin series:

$$F(y) = F(0) - \frac{y^{D-3}}{2(D-3)} + \mathcal{O}(y^{2D-7}).\qquad(33)$$

By requiring R to agree with r at spatial infinity $r \to \infty$, the integration constant R_c is chosen to be

$$R_c = r_g e^{-F(0)}.\qquad(34)$$

Then the relation between R and r is found to be

$$R \simeq r\left[1 - \frac{1}{2(D-3)}\left(\frac{r_g}{r}\right)^{D-3}\right] \quad \text{for } r \gg r_g.\qquad(35)$$

From Eqs. (27) and (35), the asymptotic behavior of the conformal factor ψ is given by

$$\psi \simeq 1 + \frac{1}{4}\left(\frac{r_g}{R}\right)^{D-3} \quad \text{for } R \gg r_g,\qquad(36)$$

which is the well-known relation for $D = 4$.

Next, we investigate the asymptotic behavior of R in the neighborhood of $r = r_{\text{lim}}$. Because $f(x; T_\infty) = 0$ has the degenerate double root at $x = x_{\text{lim}}$ given by Eq. (23), $f(x; T_\infty)$ is written in the form

$$f(x; T_\infty) = (x_{\text{lim}} - x)^2 h(x).\qquad(37)$$

Here a function $h(x)$ is a positive definite polynomial of x for $0 < x \le x_{\text{lim}}$. By substituting Eq. (37) into Eq. (30), the function $I(r)$ is rewritten in the following form:

$$I(r) := \int_{r_g/r}^1 \frac{dx}{x(x_{\text{lim}} - x)\sqrt{h(x)}}$$

$$= \frac{1}{x_{\text{lim}}\sqrt{h(x_{\text{lim}})}} \ln\left|\frac{r - r_{\text{lim}}}{r(1 - r_{\text{lim}}/r_g)}\right| + H(r_g/r),\quad(38)$$

where

$$H(y) := \frac{1}{x_{\text{lim}}\sqrt{h(x_{\text{lim}})}} \int_y^1 dx \frac{x_{\text{lim}}\sqrt{h(x_{\text{lim}})} - x\sqrt{h(x)}}{x(x_{\text{lim}} - x)\sqrt{h(x)}}.$$
$$(39)$$

Note that $H(y)$ is finite at $y = x_{\text{lim}}$. By taking the second derivative of Eq. (37), we have

$$h(x_{\text{lim}}) = \frac{1}{2}\frac{d^2 f}{dx^2}\bigg|_{x=x_{\text{lim}}}$$

$$= \frac{1}{2}(D-1)(D-3)\left[\frac{2(D-2)}{D-1}\right]^{(D-5)/(D-3)}.\quad(40)$$

Substituting this expression with Eq. (23) into Eq. (38) and using Eq. (29), we obtain the relation between R and r in the neighborhood of $r = r_{\text{lim}}$:

$$R \simeq R_0 \left(\frac{r}{r_{\text{lim}}} - 1 \right)^{1/\sqrt{(D-3)(D-2)}}, \tag{41}$$

where

$$R_0 = R_c e^{H(x_{\text{lim}})} \left(1 - \frac{r_{\text{lim}}}{r_g} \right)^{-1/\sqrt{(D-3)(D-2)}}. \tag{42}$$

Thus, the asymptotic behavior of the conformal factor is given by

$$\psi \simeq \left(\frac{r_{\text{lim}}}{R} \right)^{(D-3)/2} \quad \text{for } R \ll r_g. \tag{43}$$

Although the factor ψ becomes steeper near the puncture for higher dimensions, the overall conformal factor $\psi^{4/(D-3)}$ in Eq. (25) has the universal behavior $\psi^{4/(D-3)} \simeq (r_{\text{lim}}/R)^2$ for arbitrary values of D.

The above result shows that the coordinate origin $R = 0$ has a finite circumferential radius $r = r_{\text{lim}}$. By contrast, the proper length l from a point labeled with the isotropic radial coordinate R to the origin $R = 0$ is

$$l = \int_0^R \psi^{2/(D-3)}(R') dR' \sim r_{\text{lim}} \int_0^R \frac{dR'}{R'} = \infty. \tag{44}$$

This result implies that each stationary maximal hypersurface with $T = T_\infty$ has an infinitely long trumpet shape for $D \geq 4$.

B. Explicit construction for $D = 5$ and numerical evolution

In the following, we derive solutions of the stationary slice for $D = 5$ in terms of the variables of the BSSN formalism and then demonstrate that the solutions are useful for checking numerical-relativity codes based on the BSSN formalism for $D = 5$.

The fundamental variables in the BSSN formalism are different from those in the so-called standard $3 + 1$ formalism [28]. In the standard $3 + 1$ formalism, the fundamental quantities are the intrinsic metric γ_{ij}, the extrinsic curvature K_{ij}, the lapse function α, and the shift vector β^i ($i, j = 1, \ldots, D - 1$ in D dimensions). The initial values of these quantities are provided by solving the constraint equations, and the subsequent evolution is achieved by solving the evolution equations in certain coordinate conditions (see e.g. Ref. [29]). The standard $3 + 1$ formalism prohibits a long-term stable numerical evolution, because constraint violation modes grow in the presence of truncation error. In the BSSN formalism, the number of dynamical variables is increased to suppress the source of such instability and to enable long-term stable simulation.

The original form of the BSSN formalism was described in Refs. [8,9], and it was extended for general dimensionalities in Ref. [21]. The definitions of dynamical variables in the D-dimensional BSSN formalism are χ, the conformal factor; $\tilde{\gamma}_{ij}$, the conformal intrinsic metric; K, the trace of the extrinsic curvature; $\tilde{A}_{ij}$, a trace-free extrinsic curvature; and $\tilde{\Gamma}^i$, an auxiliary $D - 1$ variable. χ and $\tilde{\gamma}_{ij}$ are defined by

$$\tilde{\gamma}_{ij} = \chi \gamma_{ij}, \tag{45}$$

where χ is determined so that the determinant of $\tilde{\gamma}_{ij}$ is equal to unity (note that we assume to use the Cartesian coordinates). The trace-free extrinsic curvature is defined by

$$\tilde{A}_{ij} := \chi \left(K_{ij} - \frac{1}{D-1} \gamma_{ij} K \right), \tag{46}$$

and $\tilde{\Gamma}^i$ is defined by

$$\tilde{\Gamma}^i := -\frac{\partial \tilde{\gamma}^{ij}}{\partial x^j}, \tag{47}$$

where $\tilde{\gamma}^{ij}$ is the inverse of $\tilde{\gamma}_{ij}$, i.e., $\tilde{\gamma}^{ik}\tilde{\gamma}_{kj} = \delta^i_j$. The variables $\chi, K, \tilde{\gamma}_{ij}, \tilde{A}_{ij}$, and $\tilde{\Gamma}^i$ are evolved, imposing gauge conditions for α and β^i.

For a numerical-relativity simulation, the data of the stationary slice are prepared in the Cartesian spatial coordinates (x, y, z, w). In the assumption that the intrinsic metric γ_{ij} is conformally flat, $\tilde{\gamma}_{ij} = \delta_{ij}$ and $\tilde{\Gamma}^i = 0$. Furthermore, the maximal slicing condition gives $K = 0$. Since the slice is spherically symmetric, it is sufficient to prepare the data on the x axis, i.e., $y = z = w = 0$, on which the following relations hold:

$$\beta^x = \beta^R, \qquad \beta^y = \beta^z = \beta^w = 0, \tag{48}$$

$$\tilde{A}_{yy} = \tilde{A}_{zz} = \tilde{A}_{ww} = -\tfrac{1}{3}\tilde{A}_{xx} = -\tfrac{1}{3}\tilde{A}_{RR}, \tag{49}$$

$$\tilde{A}_{ij} = 0 \quad \text{for } i \neq j. \tag{50}$$

Here $R = (x^2 + y^2 + z^2 + w^2)^{1/2}$ indicates the isotropic radial coordinate. This implies that the data only for α, β^R, $\tilde{A}_{RR}$, and χ are needed in the spherical-polar coordinates.

For $D = 5$, it is easy to perform integral in Eq. (30) to give

$$R = \frac{r}{6} \left(3 + \sqrt{3[(r_g/r)^2 + 3]} \right) \times \left(\frac{(5 + 2\sqrt{6})[3 - 2(r_g/r)^2]}{2(r_g/r)^2 + 15 + 6\sqrt{2[(r_g/r)^2 + 3]}} \right)^{1/\sqrt{6}}. \tag{51}$$

The conformal factor χ, the lapse function α, and the R component of the shift vector are given, respectively, by

$$\chi = \psi^{-2} = (R/r)^2, \tag{52}$$

$$\alpha = \sqrt{1 - \left(\frac{r_g}{r} \right)^2 + \frac{4}{27} \left(\frac{r_g}{r} \right)^6}, \tag{53}$$

and

$$\beta^R = \frac{dR}{dr} \gamma^{-1} \beta = \frac{2}{3\sqrt{3}} \frac{r_g^3 R}{r^4}. \tag{54}$$

The RR component of the trace-free extrinsic curvature is

$$\tilde{A}_{RR} = -\frac{2}{\sqrt{3}} \frac{r_g^3}{r^4}. \tag{55}$$

To describe the data in the isotropic radial coordinate R, we have to give r as a function of R. Since the inversion of Eq. (51) cannot be done analytically, we numerically derive the relation $r = r(R)$ and then generate the data as functions of R. The analytic initial values of α, β^x, $\tilde{A}_{yy}$, and χ on the x axis are depicted by the solid curves in Fig. 3. Here we adopt $r_g/2$ as the unit of the length.

We evolve the initial data by using the numerical code recently developed [21] and show that the data indeed remain stationary in the puncture gauge conditions. We adopt a dynamical time slicing condition

$$\partial_t \alpha = -2\alpha K. \tag{56}$$

This is a simplified version of the $1 + \log$ slicing condition [27] that was studied in Ref. [25]. As the spatial gauge coordinates, we adopt the Γ-driver condition [24]

$$\partial_t \beta^i = \frac{D-1}{2(D-2)} B^i \quad \text{and} \quad \partial_t B^i = \partial_t \tilde{\Gamma}^i - \eta B^i, \tag{57}$$

where η is a constant. The value of η is varied over the range $1/5 r_g - 20/r_g$.

The stationary maximal slicing with the isotropic spatial coordinate satisfies the coordinate conditions (56) and (57), and, thus, the numerical data have to be unchanged during numerical evolution with these gauge conditions, if the initial data for χ, $\tilde{\gamma}_{ij}$, K, $\tilde{A}_{ij}$, α, and β^i agree with those of the stationary maximal hypersurface with $T = T_\infty$ covered by the isotropic coordinate system, together with further initial data $B^i = 0$. Therefore, the analytic solution for these variables given here is used for a test simulation of numerical-relativity codes based on the BSSN formalism and puncture gauge.
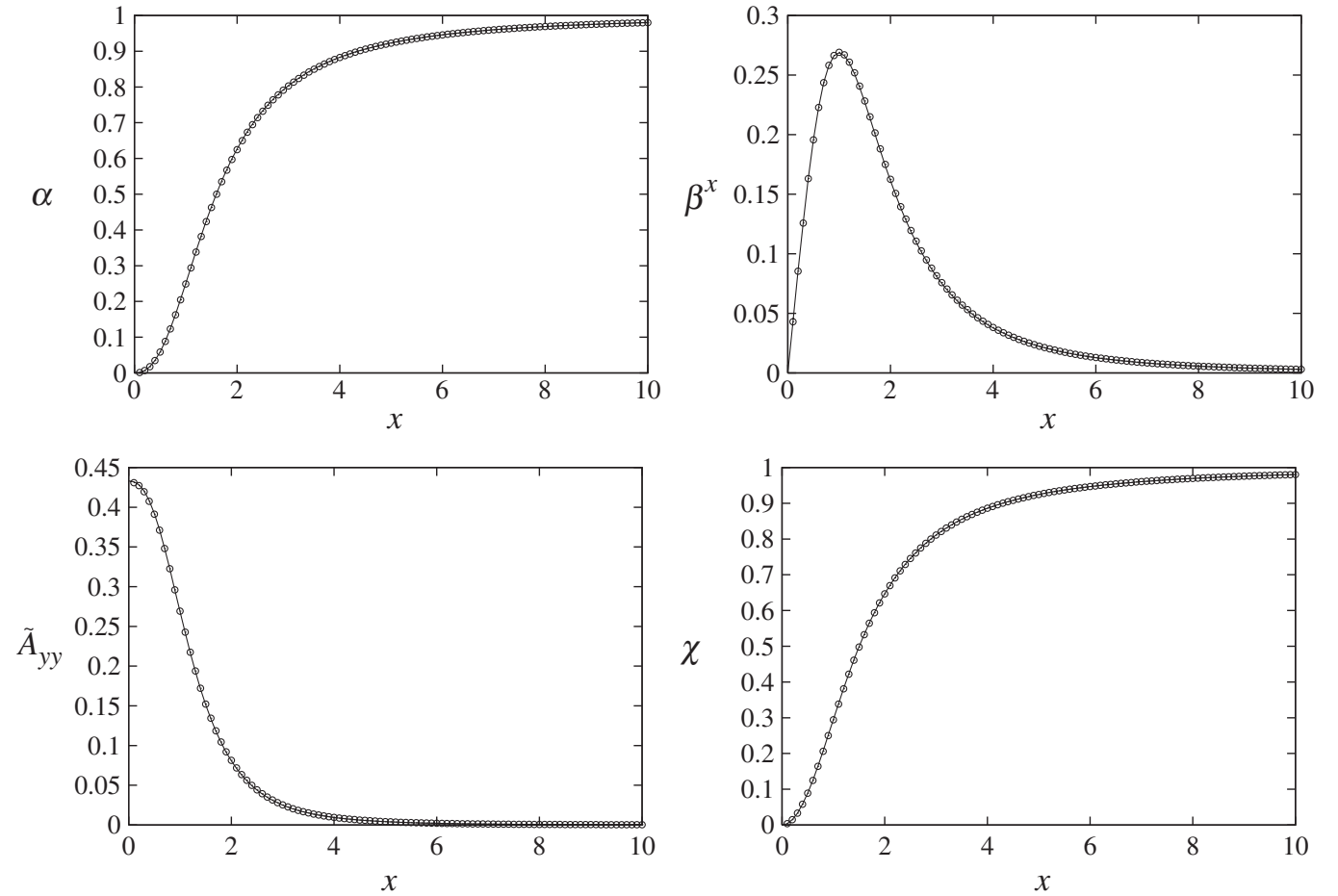

FIG. 3. The values of α, β^x, $\tilde{A}_{yy}$, and χ on the x axis for the stationary maximal hypersurface with $T = T_\infty$ (solid curves), and the data after a long-term evolution by the time $t = 100$ (⊙), where the stationary maximal hypersurface was adopted as the initial data. The units of the length and time are $r_g/2$. The data remain approximately stationary after the long-term evolution.
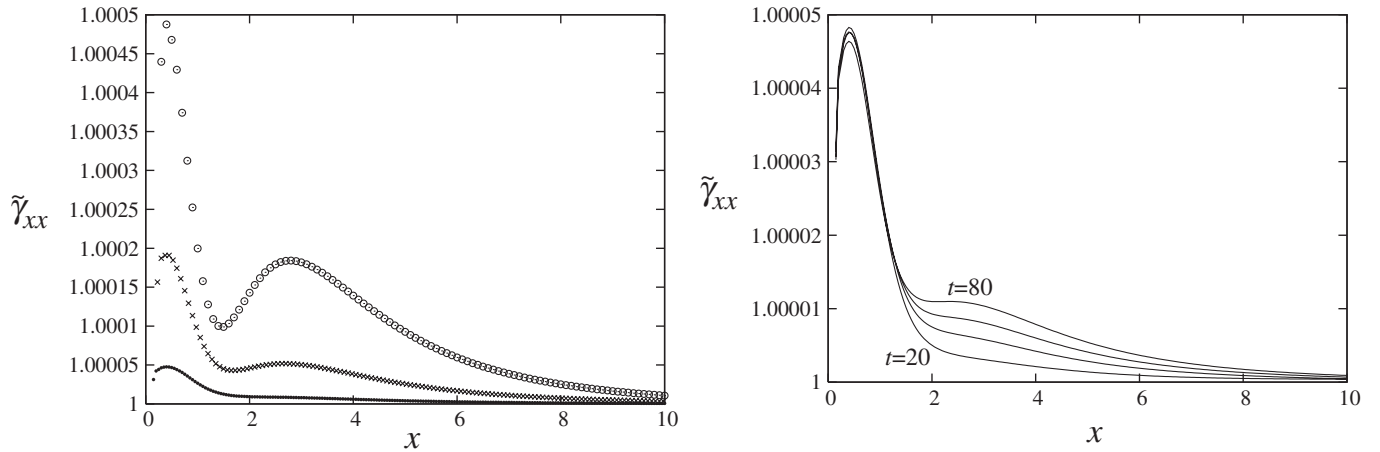
FIG. 4.   Left panel: The value of $\tilde{\gamma}_{xx}$ at time $t = 60$ for resolutions $\Delta x = 0.1$ (⊙), 0.075 (×), and 0.05 (•). The deviation from the analytic solution $\tilde{\gamma}_{xx}^{(a)} = 1$ becomes smaller as the resolution is increased. Right panel: Snapshots of $\tilde{\gamma}_{xx}$ for a fixed grid spacing $\Delta x = 0.05$ for time $t = 20$, 40, 60, and 80. The error gradually increases during the evolution.

The data obtained by evolving the above analytic initial data with $B^i = 0$ are depicted by the circles ⊙ in Fig. 3. In the numerical simulation, the outer boundary is located at a sufficiently distant zone ($x = 200$), and the grid size is uniformly $\Delta x = 0.1$. The value of η is chosen for a wide range as $\eta = 1/(5r_g) - 20/r_g$, and we confirm that the result does not depend on the choice (but we found that numerical error becomes large for very large values of η). Figure 3 shows that the numerical data at $t = 100$ agree well with the initial data $t = 0$. Thus, we conclude that the numerical data remain approximately stationary and unchanged in time.

The left panel of Fig. 4 shows the evolution of numerical values of $\tilde{\gamma}_{xx}$ on the x axis obtained by $\eta = 2/r_g$ for several grid resolutions with $\Delta x = 0.1$, 0.075, and 0.05. Because the analytic solution is $\tilde{\gamma}_{xx}^{(a)} = 1$, the deviation from unity indicates the amount of the error. This figure clearly shows that the deviation is decreased as the resolution is increased, and, hence, the deviation from the analytic data is caused only by the numerical error. Indeed, the values of averaged error are 0.01%, 0.003%, and 0.0008% for $\Delta x = 0.1$, 0.075, and 0.05, respectively. Here the spatial pattern of the error for a fixed time t with $t \gg 10r_g$ was found to depend on the grid resolutions. However, as the resolution is increased, the pattern becomes less dependent on the resolution and the error decreases approximately at the fourth order. This implies that our numerical solution achieves the four-order convergence in the limit $\Delta x \to 0$ except at the region near the puncture (where the analyticity of solution is broken and the numerical solution should not converge at the fourth order). The right panel shows the snapshots of $\tilde{\gamma}_{xx}$ for $t = 20$–80 for the grid size $\Delta x = 0.05$. Although the error grows during the evolution, the growth rate is small. In fact, the amount of increase in the averaged error between $t = 20$ and 80 is 0.0003%. These results illustrate both the

accuracy of our numerical simulations and the effectiveness of the foliation by the stationary maximal hypersurfaces as a benchmark for checking a five-dimensional numerical-relativity code.

V. SUMMARY

We have studied the foliation of the D-dimensional Schwarzschild-Tangherlini spacetime by the two kinds of one-parameter family of maximal hypersurfaces: the reflection-symmetric foliation with respect to the wormhole slot and the stationary foliation. We have shown that both foliations avoid the singularity for $D \geq 5$, as in the case of $D = 4$. It is also shown that each hypersurface of the stationary foliation has an infinitely long trumpetlike shape in the neighborhood of the black-hole puncture located at the origin of the isotropic coordinate. Because the stationary foliation is the attractor of the numerical evolution by a dynamical slicing condition [25], both the maximal slicing condition and the dynamical slicing conditions will have the preferable nature for the puncture method for $D \geq 4$. We presented the explicit solution of the stationary foliation for $D = 5$ and showed, by performing the numerical simulation, that it is useful for a benchmark test of $D = 5$ numerical-relativity codes.

The remaining issues to be explored are as follows. Although we expect that the puncture gauge condition based on a dynamical slicing and Γ-driver gauge condition also works well for many issues in the higher-dimensional numerical relativity, as demonstrated in Ref. [30] in the four-dimensional case, more detailed studies for a variety of spacetimes are obviously needed. For example, it is important to figure out the gauge conditions suitable for simulating higher-dimensional rotating black-hole spacetimes (i.e., Myers-Perry black holes [31]) and for simulating black holes with high velocity. These are issues to be studied.

ACKNOWLEDGMENTS

The authors thank colleagues in the theoretical astrophysics and gravity group in Osaka City University. H. Y. is supported by JSPS. M. S. was in part supported by Grant-in-Aid for Scientific Research (No. 21340051) and by Grant-in-Aid for Scientific Research on Innovative Area (No. 20105004) of the Japanese Monbukagakusho.

APPENDIX: KRUSKAL EXTENSION AND EMBEDDING OF MAXIMAL HYPERSURFACES

In this section, we analyze the Kruskal extension of the *D*-dimensional Schwarzschild-Tangherlini spacetime and explain how to embed maximal hypersurfaces in it. We start from the standard metric (14) in the static coordinates (τ, r) and consider the region $r > r_g$. First, we introduce the so-called tortoise coordinate r_*:

$$r_* := \int \frac{dr}{1 - (r_g/r)^{D-3}}$$
$$= r + \frac{r_g}{D-3}\left[\ln\left| \frac{r}{r_g} - 1 \right| + G(r) \right]. \quad (A1)$$

Here, defining

$$G_n(r) := \cos\left(\frac{2n\pi}{D-3}\right) \ln\left| \left(\frac{r}{r_g}\right)^2 - \frac{2r}{r_g}\cos\left(\frac{2n\pi}{D-3}\right) + 1 \right|$$
$$+ 2\sin\left(\frac{2n\pi}{D-3}\right)$$
$$\times \arctan\left(\frac{\cos[2n\pi/(D-3)] - r/r_g}{\sin[2n\pi/(D-3)]}\right), \quad (A2)$$

the function $G(r)$ is given by

$$G(r) = \sum_{n=1}^{(D-4)/2} G_n(r), \quad \text{for even } D \geq 4, \quad (A3)$$

and

$$G(r) = \ln\left| \frac{r}{r_g} + 1 \right|^{-1} + \sum_{n=1}^{(D-5)/2} G_n(r), \quad \text{for odd } D \geq 5. \quad (A4)$$

It is easily seen that $G(r)$ is regular for $r \geq 0$. Then we introduce the Kruskal null coordinates as

$$U = -r_g \exp[-(D-3)(\tau - r_*)/2r_g], \quad (A5)$$

$$V = +r_g \exp[+(D-3)(\tau + r_*)/2r_g]. \quad (A6)$$

In these coordinates, the metric (14) is reduced to the following form:

$$ds^2 = -\left(\frac{2}{D-3}\right)^2 e^{-(D-3)r/r_g - G(r)} \sum_{n=1}^{D-3}\left(\frac{r_g}{r}\right)^n dUdV$$
$$+ r^2 d\Omega_{D-2}^2. \quad (A7)$$

Now we can extend the spacetime in a similar manner to the four-dimensional case. The coordinates U and V introduced by Eqs. (A5) and (A6) are restricted to the region $U < 0$ and $V > 0$. However, since the metric is regular at $U = 0$ and $V = 0$, the spacetime is extended to the region $U > 0$ or $V < 0$. The maximally extended spacetime consists of four regions, and the three regions obtained by the extension are the black-hole region $U > 0$ and $V > 0$, the white-hole region $U < 0$ and $V < 0$, and the other region $U > 0$ and $V < 0$ outside of the two holes beyond the wormhole slot. The relation between the coordinates (U, V) and the static coordinates (t, r) in each extended region is given by appropriately changing the sign of Eqs. (A5) and (A6). Note that the range of r is $0 < r < r_g$ in the black- and white-hole regions, while $r_g < r$ in the two outside regions. The line element (A7) is regular everywhere except at the two physical curvature singularities, $r = 0$, in the black and white holes. See Fig. 2 for the structure of the maximally extended spacetime.

In order to embed maximal hypersurfaces in the Kruskal diagram, we consider the coordinate transformation between the Kruskal coordinates (U, V) and the coordinates (t, r) for maximal slicing. Since (U, V) and (τ, r) are related through Eqs. (A5) and (A6) whereas (τ, r) and (t, r) are related through Eqs. (15) and (16), we obtain

$$\left.\frac{\partial U}{\partial r}\right|_t = \frac{D-3}{2r_g}\left[1 - \left(\frac{r_g}{r}\right)^{D-3}\right]^{-1}(1 + \gamma^{1/2}Tr^{-(D-2)})U,$$
$$(A8)$$

$$\left.\frac{\partial V}{\partial r}\right|_t = \frac{D-3}{2r_g}\left[1 - \left(\frac{r_g}{r}\right)^{D-3}\right]^{-1}(1 - \gamma^{1/2}Tr^{-(D-2)})V.$$
$$(A9)$$

Once the arbitrary function of integration $T(t)$ is determined, we obtain a maximal hypersurface in the Kruskal diagram by integrating these two equations.

---

[1] F. Pretorius, Phys. Rev. Lett. **95**, 121101 (2005).
[2] M. Campanelli, C. O. Lousto, P. Marronetti, and Y. Zlochower, Phys. Rev. Lett. **96**, 111101 (2006).
[3] J. G. Baker, J. Centrella, D. I. Choi, M. Koppitz, and J. van

Meter, Phys. Rev. Lett. **96**, 111102 (2006).
[4] F. Herrmann, D. Shoemaker, and P. Laguna, arXiv:gr-qc/0601026.
[5] U. Sperhake, Phys. Rev. D **76**, 104015 (2007).

[6] M. A. Scheel, H. P. Pfeiffer, L. Lindblom, L. E. Kidder, O. Rinne, and S. A. Teukolsky, Phys. Rev. D **74**, 104006 (2006).

[7] B. Brügmann, J. A. González, M. Hannam, S. Husa, U. Sperhake, and W. Tichy, Phys. Rev. D **77**, 024027 (2008).

[8] M. Shibata and T. Nakamura, Phys. Rev. D **52**, 5428 (1995).

[9] T. W. Baumgarte and S. L. Shapiro, Phys. Rev. D **59**, 024007 (1998).

[10] T. Banks and W. Fischler, arXiv:hep-th/9906038.

[11] S. Dimopoulos and G. Landsberg, Phys. Rev. Lett. **87**, 161602 (2001).

[12] S. B. Giddings and S. Thomas, Phys. Rev. D **65**, 056010 (2002).

[13] N. Arkani-Hamed, S. Dimopoulos, and G. R. Dvali, Phys. Lett. B **429**, 263 (1998); I. Antoniadis, N. Arkani-Hamed, S. Dimopoulos, and G. R. Dvali, *ibid.* **436**, 257 (1998).

[14] L. Randall and R. Sundrum, Phys. Rev. Lett. **83**, 3370 (1999).

[15] P. Kanti, Lect. Notes Phys. **769**, 387 (2009).

[16] U. Sperhake, V. Cardoso, F. Pretorius, E. Berti, and J. A. González, Phys. Rev. Lett. **101**, 161101 (2008).

[17] M. Shibata, H. Okawa, and T. Yamamoto, Phys. Rev. D **78**, 101501(R) (2008).

[18] U. Sperhake, V. Cardoso, F. Pretorius, E. Berti, T. Hinderer, and N. Yunes, Phys. Rev. Lett. **103**, 131102 (2009).

[19] H. Yoshino and Y. Nambu, Phys. Rev. D **67**, 024009 (2003).

[20] H. Yoshino and V. S. Rychkov, Phys. Rev. D **71**, 104028 (2005).

[21] H. Yoshino and M. Shibata, arXiv:0907.2760 [Phys. Rev. D (to be published)].

[22] F. R. Tangherlini, Nuovo Cimento **27**, 636 (1963).

[23] F. Estabrook, H. Wahlquist, S. Christensen, B. DeWitt, L. Smarr, and E. Tsiang, Phys. Rev. D **7**, 2814 (1973).

[24] M. Alcubierre, B. Brügmann, P. Diener, M. Koppitz, D. Pollney, E. Seidel, and R. Takahashi, Phys. Rev. D **67**, 084023 (2003).

[25] M. Hannam, S. Husa, B. Brügmann, J. A. González, U. Sperhake, and N. Ó. Murchadha, J. Phys. Conf. Ser. **66**, 012047 (2007).

[26] T. W. Baumgarte and S. L. Shapiro, Phys. Rev. D **59**, 024007 (1998).

[27] C. Bona, J. Massó, E. Seidel, and J. Stela, Phys. Rev. D **56**, 3405 (1997).

[28] J. W. York, Jr., in *Sources of Gravitational Radiation*, edited by L. L. Smarr (Cambridge University Press, Cambridge, England, 1979), p. 83.

[29] L. Smarr and J. W. York, Jr., Phys. Rev. D **17**, 2529 (1978).

[30] M. Hannam, S. Husa, D. Pollney, B. Brügmann, and N. Ó Murchadha, Phys. Rev. Lett. **99**, 241102 (2007).

[31] R. C. Myers and M. J. Perry, Ann. Phys. (N.Y.) **172**, 304 (1986).